The Astrophysical Journal, 990:54 (10pp), 2025 September 1 https://doi.org/10.3847/1538-4357/adf3b1

The Small Separation A-star Companion Population: Tentative Signatures of Enhanced Multiplicity with Primary Mass

Matthew De Furio[1,2], Tyler Gardner[3], John D. Monnier[4], Michael R. Meyer[4], Kaitlin M. Kratter[5], Cyprien Lanthermann[6], Narsireddy Anugu[6], Stefan Kraus[3], and Benjamin R. Setterholm[4,7]
[1] Department of Astronomy, The University of Texas at Austin, 2515 Speedway, Stop C1400, Austin, TX 78712, USA; defurio@utexas.edu
[2] NSF Astronomy and Astrophysics Postdoctoral Fellow
[3] Astrophysics Group, Department of Physics and Astronomy, University of Exeter, Stocker Road, Exeter, EX4 4QL, UK
[4] Department of Astronomy, University of Michigan, Ann Arbor, MI 48109, USA
[5] Department of Astronomy and Steward Observatory, University of Arizona, Tucson, AZ, USA
[6] The CHARA Array of Georgia State University, Mount Wilson Observatory, Mount Wilson, CA 91203, USA
[7] Max-Planck-Institut für Astronomie, Heidelberg, DE, Germany
Received 2025 May 18; revised 2025 July 6; accepted 2025 July 22; published 2025 August 25

Abstract

We present updated results from our near-infrared long-baseline interferometry (LBI) survey to constrain the multiplicity properties of intermediate-mass A-type stars within 80 pc. Previous adaptive optics surveys of A-type stars are incomplete at separations <20 au. Therefore, an LBI survey allows us to explore separations previously unexplored. Our sample consists of 54 A-type primaries with estimated masses between 1.44 and 2.93$M_{\odot}$ and ages 10–790 Myr, which we observed with the Michigan Infra-Red Combiner-eXeter and Michigan Young Star Imager at Center for High Angular Resolution Astronomy instruments at the Center for High Angular Resolution Astronomy Array. We use the open source software CANDID to detect two new companions, seven in total, and we performed a Bayesian demographic analysis to characterize the companion population. We find the separation distribution consistent with being flat, and we estimate a power-law fit to the mass ratio distribution with index $-0.13^{+0.92}_{-0.95}$ and a companion frequency of $0.25^{+0.17}_{-0.11}$ over mass ratios 0.1–1.0 and projected separations 0.01–27.54 au. We find a posterior probability of 0.53 and 0.04 that our results are consistent with extrapolations based on previous models of the solar-type and B-type companion population, respectively. Our results suggest that the close companion population to A-type stars is comparable to that of solar-type stars and that close companions to B-type stars are potentially more frequent, which may be indicative of increased disk fragmentation for stars $\gtrsim 3M_{\odot}$.

Unified Astronomy Thesaurus concepts: Binary stars (154); Multiple stars (1081); A stars (5); Star formation (1569); Stellar physics (1621); Long baseline interferometry (932); Bayesian statistics (1900)

1. Introduction

The majority of Sun-like stars in the Galaxy have a stellar companion (D. Raghavan et al. 2010; M. Moe & R. Di Stefano 2017). The same may be true of low-mass M-type stars, the most common type of star, when also considering brown dwarf companions (J. G. Winters et al. 2019; N. Susemiehl & M. R. Meyer 2022). The ubiquity of companions over a broad range of stars is a result of the star formation process. Companions form at early times ($\lesssim$1 Myr) and exist in stable configurations across orders of magnitude in primary mass (O-stars to brown dwarfs), orbital separation (<1–1000s au), and mass ratios.

Companions to stars are believed to be predominantly produced through two common channels, disk fragmentation and turbulent fragmentation, resulting in various mass ratios and orbital separations as a function of host star mass. Disk fragmentation results in companions at separations less than the size of the disk, 100 au (F. C. Adams et al. 1989; I. A. Bonnell & M. R. Bate 1994), while turbulent fragmentation of molecular cloud cores generates gravitationally bound companions out to 1000s of au (S. P. Goodwin et al. 2004; S. S. R. Offner et al. 2010). Subsequent processes can alter their separations through migration and cluster dynamics, and mass ratios through preferential accretion onto the companion (M. R. Bate et al. 2002, 2003; M. D. Young & C. J. Clarke 2015; S. S. R. Offner et al. 2023). These processes can significantly affect circumstellar disk evolution, planet formation, and allowable planetary architectures (A. L. Kraus et al. 2016; M. Moe & K. M. Kratter 2021). The outcomes of multiple formation place substantial constraints on star and planet formation theory, and a thorough understanding of multiplicity is necessary to develop a comprehensive theory of star formation.

Previous multiplicity surveys in the Galactic field demonstrate that the companion frequencies and distributions of mass ratio (M_2/M_1) and orbital separation depend on primary mass (S. S. R. Offner et al. 2023). They find that the companion separation distribution can be modeled as a lognormal distribution with a peak at 6 au for brown dwarfs (I. N. Reid et al. 2006), 20 au for M-type primaries (M. Janson et al. 2012; J. G. Winters et al. 2019), and 50 au for solar-type primaries (D. Raghavan et al. 2010). Higher mass O and B stars appear to have separation distributions flat in log-space (M. Moe & R. Di Stefano 2017), with high frequencies of companions across all separations (S. S. R. Offner et al. 2023). A-type primaries (1.5–2.5$M_{\odot}$) appear to have a peak around 390 au (R. J. De Rosa et al. 2014). However, this is based on a

multiplicity survey that suffers from incompleteness for separations <20 au, leaving open the possibility for a significant population of close separation companions to A-type primaries (M. Moe & R. Di Stefano 2017).

The radial velocity (RV) survey of J. M. Carquillat & J. L. Prieur (2007) of Am stars, chemically peculiar A-stars with small rotational velocities, found a different peak of very close companions with a mean period of 5 days (0.1 au). Due to their small rotational velocity, these chemically peculiar A-stars are biased toward close companions that may reduce the rotational velocity of the primary, and therefore are not representative of all A-type stars. A similar peak has been identified for O-type primaries (H. Sana et al. 2012), while a recent long-baseline interferometry survey finds a preference for companions near 10 au although potentially biased against closer companions (C. Lanthermann et al. 2023). RV surveys of chemically typical A-type stars are difficult, as they are usually fast rotators and have broad absorption lines, as opposed to the overwhelmingly slow rotational velocities of chemically peculiar A-type stars. Therefore, this type of survey has not been performed to date. In M. De Furio et al. (2022a; hereafter DF22), we observed 27 typical A-type stars with LBI at the Center for High Angular Resolution Astronomy (CHARA) Array (T. A. ten Brummelaar et al. 2016) and found a handful of close companions. This sample is quite small and suffers from large error bars. Therefore, the close companion population around typical A-type stars is still underexplored. Expanding upon this sample is necessary to probe the impact of primary mass on the formation and evolution of close binary systems and filling in the gap in our understanding between solar-type and OB-type multiplicity.

In this paper, we present the results of our expanded survey, including new observations and an updated Bayesian demographic analysis. In Section 2, we describe the newly observed data and the methods to identify companions. In Section 3, we present the companion detections, describe our detection limits, and characterize the close companion population of A-type primary stars with a Bayesian analysis. In Section 4, we compare our results to various multiplicity surveys and discuss the implications. In Section 5, we summarize our conclusions.

2. Methods

2.1. Observations

As a continuation of our A-star survey, we observed 30 additional chemically typical A-type stars over the course of four nights (UT 2022 May 6–8 and July 30) at the CHARA Array (T. A. ten Brummelaar et al. 2005), an optical and near-infrared interferometric array consisting of six 1 m telescopes with baselines up to 331 m. All sources were observed over the H band with the grism mode (R 190) on the Michigan Infra-Red Combiner-eXeter (MIRC-X) instrument (J. D. Monnier et al. 2006; N. Anugu et al. 2020) and some over the K-band with the prism mode (R 50) on the Michigan Young Star Imager at CHARA (MYSTIC) instrument (J. D. Monnier et al. 2018; B. R. Setterholm et al. 2023) once it became available to the public, see Table 1. The higher spectral resolution of MIRC-X allows us to identify companions at wider separations, out to roughly 0.″3 (N. Anugu et al. 2020), while MYSTIC is used to confirm marginal detections and obtain color information on each detected companion. We also employed the etalon to properly calibrate the wavelength, see T. Gardner et al. (2021). A typical observing sequence follows 10 minutes source integration, the standard shutters sequence (N. Anugu et al. 2020), and repeated 10 minutes source integration. For some bright primaries, we instead do 5+5 minutes source integrations for a comparable signal-to-noise ratio to all other targets. We opted to observe no calibrator stars as the majority of targets in our previous run were identified as single stars. Therefore, we use science targets well fit by a single star model to serve as calibrators to stars observed close in time, see Table 2.

2.2. Data Reduction and Analysis

We followed the same data reduction steps as DF22 and summarized them here. We used the standard MIRC-X data pipeline (version 1.3.3, N. Anugu et al. 2020) to measure the visibilities, closure phases, and differential phases from each baseline pair in the raw interferometric data. We used the default reduction parameters and set coherent integration frames (ncoh) to 10 and maximum integration time to 60 s to allow for wide companion detection. For final calibration, we used a modified version of the MIRC-X and original MIRC pipeline (J. D. Monnier et al. 2007; M. Zhao et al. 2009; X. Che et al. 2011; J. D. Monnier et al. 2012) to filter out bad quality data by applying various quality checks, producing more reliable sensitivity maps (e.g., T. Gardner et al. 2021).

We also followed the same data analysis routine as DF22 and summarized it here. We utilized the open source Python code CANDID (A. Gallenne et al. 2015) to identify companions and define sensitivity limits to all of the sources in our sample from their measured interferometric observables, see R. C. Jennison (1958), A. E. E. Rogers et al. (1974), J. D. Monnier (2000), J. D. Monnier et al. (2004) for a description of these interferometric parameters. With CANDID, we fit single and binary star models to the closure phases measured for each source in order to identify companions because this interferometric observable is most sensitive to the presence of companions. For sources with companions, we then ran a more thorough analysis on the closure phases and squared visibilities to properly model the astrophysical scene, the results of which are displayed in Table 3. We assume a uniform disk diameter in our model of both the primary and the secondary. Some of these sources are likely rapid rotators, which would make them elongated if resolved, and the assumption of a uniform disk is too simplistic. Even in this case, the best-fit χ^2_ν values to the detected companions still demonstrate that the model well represents the data. Additionally, for all companion detections, we divide by a correction factor of 1.00535 to the fitted separation to bring the data to an absolute wavelength scale (T. Gardner et al. 2022) with the corrected values in Table 3.

3. Results

3.1. Detections

We detected two new companions out of the 30 additional A-type stars in our sample, HD 205835 and HD 210715. Both detections had a significance of 8σ, the maximum permitted value in CANDID, indicative of strong detections. These companions were detected at projected separations of 16.631 and 157.296 mas (physical separation of 1.120 and 8.747 au) with flux ratios = 31.3 and 3.4%, respectively, see Table 3. We estimated the masses of both new companions using the

Table 1
Table of Sources Observed with MIRC-X and MYSTIC

HD Number	HIP Number	SpType	Distance (pc)	Age (Myr)	Mass ($M_\odot$)	Date Observed MJD	SNR Acceleration (Kervella+22)	Gaia NSS Code
1404[a,b]	1473	A2V	$43.00^{+0.34}_{-0.33}$	200	2.26	59790.43	1.16	None
4058[a,b]	3414	A5V	$54.77^{+3.39}_{-0.65}$	250	1.9	59790.45	1.47	tbosb2
5448	4436	A5V	$42.37^{+0.11}_{-0.19}$	450	2.39	59203.08	1.82	None
11636[c]	8903	A5V	$18.27^{+0.25}_{-0.25}$	630	2.01	59204.08	N/A	None
14055[a,b]	10670	A1Vnn	$35.74^{+0.60}_{-0.58}$	100	2.57	59790.48	1.19	None
15550	11678	A9V	$71.77^{+1.84}_{-0.56}$	790	1.84	59204.14	1.28	None
20677	15648	A3V	$48.11^{+0.30}_{-0.25}$	250	2.11	59203.18	1.20	None
21912	16591	A3V	$56.29^{+0.16}_{-0.15}$	40	1.77	59203.16	0.77	tbosb1
24809	18547	A8V	$63.76^{+0.12}_{-0.11}$	100	1.7	59203.22	4.34	None
28910	21273	A8V	$46.97^{+0.38}_{-0.37}$	630	2.21	59204.22	1.00	tbootsc
29388[c]	21589	A6V	$47.1^{+1.2}_{-1.2}$	630	2.17	59204.19	4.99	None
31647[a]	23179	A1V	$49.91^{+0.29}_{-0.29}$	30	2.39	59508.56	0.85	None
32301	23497	A7V	$57.55^{+4.80}_{-1.87}$	630	2.22	59204.25	0.59	None
46089[c]	31119	A3V	$63.7^{+1.5}_{-1.5}$	560	2.2	59203.29	1.19	None
48097[c]	32104	A2V	$43.6^{+1.3}_{-1.3}$	30	1.94	59203.32	0.58	None
56537[c]	35350	A3V	$30.9^{+0.2}_{-0.2}$	320	2.39	59204.28	0.90	None
59037	36393	A4V	$55.91^{+3.84}_{-1.44}$	500	2.16	59203.35	1.44	None
66664	39567	A1V	$65.89^{+0.70}_{-0.58}$	320	2.42	59204.33	0.74	None
74198[c]	42806	A1IV	$55.6^{+0.6}_{-0.6}$	320	2.49	59204.39	1.76	None
74873	43121	A1V	$54.82^{+0.15}_{-0.14}$	50	1.88	59204.36	2.40	None
77660	44574	A8V	$78.28^{+0.20}_{-0.19}$	710	1.81	59203.43	2.26	None
84107	47701	A2IV	$51.24^{+2.38}_{-0.98}$	10	1.44	59203.45	1.16	None
92941[c]	52513	A5V	$66.9^{+1.4}_{-1.4}$	450	1.84	59204.48	1.18	None
97244	54688	A5V	$62.19^{+0.18}_{-0.15}$	60	1.72	59204.45	2.11	None
99787	56034	A2V	$69.64^{+0.68}_{-0.89}$	280	2.32	59203.48	1.43	None
106591[b]	59774	A3V	$24.86^{+0.58}_{-2.58}$	320	2.31	59706.22	0.76	tbootsc
106661	59819	A3V	$66.01^{+0.09}_{-0.21}$	400	2.29	59204.51	1.44	None
112734	63320	A5	$73.73^{+0.44}_{-0.30}$	40	1.69	59203.53	0.64	None
115271[c]	64692	A7V	$74.1^{+2.4}_{-2.4}$	560	2.1	59203.59	65.69	None
118232[b]	66234	A5V	$56.83^{+0.36}_{-0.35}$	500	2.38	59706.27	1.31	None
120047	67194	A5V	$52.84^{+0.79}_{-0.39}$	500	1.78	59204.6	0.47	None
121164	67782	A7V	$73.60^{+0.58}_{-0.44}$	500	1.97	59204.57	1.56	None
124675[b]	69483	A8IV	$49.62^{+0.27}_{-0.27}$	500	2.38	59706.31	1.32	None
125161[b]	69713	A7V	$29.86^{+0.97}_{-0.35}$	50	1.81	59706.33	0.90	None
130109[b]	72220	A0V	$43.46^{+0.45}_{-0.42}$	320	2.71	59705.32	3.06	None
141378[b]	77464	A5IV	$53.77^{+0.20}_{-0.19}$	250	2	59705.35	0.76	None
147547[b]	80170	A9III	$61.84^{+0.51}_{-0.56}$	500	2.5	59707.37	1.77	None
152107[b]	82321	A2Vspe...	$53.31^{+0.27}_{-0.27}$	400	2.31	59706.37	6.66	None
154494[b]	83613	A4IV	$42.22^{+0.20}_{-0.02}$	280	2.02	59707.41	1.29	None
156729[a,b]	84606	A2V	$52.08^{+0.07}_{-0.06}$	350	2.4	59790.18	26.46	None
158352[b]	85537	A7V	$64.03^{+0.05}_{-0.07}$	630	2.1	59705.42	2.52	None
165777[b]	88771	A4IVs	$27.72^{+4.18}_{-0.60}$	400	2.08	59705.45	1.36	None
173582[b]	XXX	A3	$48.32^{+0.96}_{-0.92}$	400	2.13	59706.41	N/A	None
173607[b]	XXX	A5	$49.17^{+0.25}_{-0.25}$	350	1.99	59706.45	N/A	None
173880[b]	92161	A5III	$27.95^{+0.04}_{-0.03}$	110	1.94	59705.48	138.42	None
174602[a,b]	92405	A3V	$74.20^{+1.55}_{-1.10}$	500	2.32	59790.22	0.94	None
177724[b]	93747	A0Vn	$26.16^{+0.24}_{-0.24}$	130	2.93	59705.51	1.18	None
184006[b]	95853	A5V	$37.54^{+0.24}_{-0.24}$	450	2.34	59706.49	1.02	None
192640[a,b]	99770	A2V	$40.74^{+0.15}_{-0.15}$	40	2.71	59790.26	2.01	None
199254[b]	103298	A4V	$61.29^{+1.31}_{-0.52}$	450	2.06	59705.53	56.40	None
204414[a,b]	105966	A1V	$60.25^{+0.39}_{-0.32}$	200	2.19	59790.3	3.13	None
205835[a,b]	106711	A5V	$67.33^{+4.37}_{-3.14}$	630	2.2	59790.33	3.24	tbootsc
210715[a,b]	109521	A5V	$55.61^{+0.65}_{-0.80}$	500	2.04	59790.37	80.77	None
213558[a,b]	111169	A1V	$31.75^{+0.20}_{-0.20}$	130	2.45	59790.39	0.69	None

Notes. Where indicated, in our full sample of 54 stars with Modified Julian Date (MJD) of observation. Listed spectral types, ages, and masses for each star were taken from R. J. De Rosa et al. (2014), who describe their method of estimating age and mass in their Appendix. Distances and their errors (16% and 84% confidence level) were extracted from the Gaia DR3 archive (Gaia Collaboration et al. 2016; C. Babusiaux et al. 2023; Gaia Collaboration et al. 2023), except where noted. Listed is the acceleration signal to noise ratio (SNR) from P. Kervella et al. (2022) that indicates deviations from the proper motion over the time baseline of Hipparcos and Gaia eDR3. Values greater than 3 are indicative of a likely companion over a broad range of potential separations and mass ratios. The nonsingle star catalog codes from Gaia DR3 are displayed, whose descriptions can be found in Gaia Collaboration (2022).

[a] Observed with both MIRC-X and MYSTIC at CHARA Array.

[b] Newly observed in this work.

[c] Distance taken from R. J. De Rosa et al. (2014) using the Hipparcos catalog (ESA 1997) due to unreliable Gaia measurements for bright stars.

Table 2
Table of Calibrators

Calibrator Name	UD Diameter (mas)		Night (UT)	UD Reference
HD 99787	0.303	0.024	2020 Dec 20	(1)
HD 44851	0.58	0.014	2020 Dec 20	(2)
HD 21912	0.276	0.007	2020 Dec 20	(2)
HD 120047	0.308	0.008	2020 Dec 21	(2)
HD 32301	0.479	0.033	2020 Dec 21	(2)
HD 74198	0.362	0.024	2020 Dec 21	(2)
HD 19066[a]	0.85	0.06	2021 Oct 21	(2)
HD 141378	0.314	0.009	2022 May 6	(2)
HD 158352	0.41	0.01	2022 May 6	(2)
HD 173880	0.47	0.05	2022 May 6	(2)
HD 124675	0.55	0.06	2022 May 7	(2)
HD 152107	0.39	0.03	2022 May 7	(2)
HD 184006	0.59	0.04	2022 May 7	(3)
HD 161868	0.57	0.04	2022 May 8	(2)
HD 174602[a]	0.36	0.01	2022 Jul 30	(2)
HD 204414[a]	0.282	0.009	2022 Jul 30	(2)
HD 14055[a]	0.47	0.033	2022 Jul 30	(3)

Notes.
[a] Observed with both MIRC-X and MYSTIC at CHARA Array. **References.** (1) S. J. Swihart et al. (2017), (2) L. Bourges et al. (2017), (3) searchcal (A. Chelli et al. 2016).

measured flux ratio of the system and the MIST evolutionary models (B. Paxton et al. 2011, 2013, 2015, 2018; J. Choi et al. 2016; A. Dotter 2016), assuming the primary mass and age from R. J. De Rosa et al. (2014). The mass ratios (q) of these systems are 0.71 and 0.34, respectively, see Table 4. Both of these targets were reported to have a proper motion anomaly using Hipparcos and Gaia catalogs that could be indicative of a companion (P. Kervella et al. 2019, 2022). Several other sources in our sample were reported as having a high proper motion anomaly but without detections with CHARA, see Table 1, either due to the suspected companion outside of our resolution range (i.e., $a \gtrsim 30$ au) or too faint given our contrast limits (i.e., $q \lesssim 0.15$). HD 11636 and HD 28910 are two binaries that we previously detected with MIRC-X in M. De Furio et al. (2022a) and were previously spectroscopically identified (H. A. Abt 1965; D. Pourbaix 2000). HD 205835 was identified in Gaia Data Release 3 (DR3) as a nonsingle star with the label "OrbitalTargetedSearch" meaning this companion was previously known and used to test the astrometric orbit fitting code (Gaia Collaboration et al. 2023; B. Holl et al. 2023). Gaia DR3 reports a period of 596 days and an eccentricity of 0.51. Given the adopted masses and period of the binary system, we estimate from Kepler's third law a semimajor axis of 2.16 au and a minimum and maximum distance from the primary as 1.06 and 3.26 au, assuming the eccentricity from Gaia. Our observed projected separation, given the distance to the source, is 1.12 au, which is within the estimated bounds. Of the other sources in our full sample, only HD 106591 was identified in Gaia DR3 as being a nonsingle star. It has an astrometrically identified companion with a period of 53 days and eccentricity of 0.45. Given its period and the distance to this source, the companion should have a semimajor axis of 0.21–0.56 au (8–23 mas), within our resolution sensitivity, but depending on the orientation of the orbit and time of observation could be unresolvable. Without a companion mass estimate, we are unable to determine whether such a source should be detectable in the interferometric data. All other sources within our sample had no companion detections in either our analysis or Gaia DR3.

For these two new detections, the squared visibilities were noisy, and it was difficult to estimate the diameters and resolved flux. Therefore, we only used the closure phases to identify companions and estimate fluxes. However, there was no impact of a resolved primary on the derived companion parameters, and thus our exclusive use of the closure phases for these two sources is appropriate, and the companion parameters are reliable.

3.2. Detection Limits

As in DF22, we used CANDID to define the limit at which we can recover true companions to each source within our sample. A thorough description is given in DF22, and we summarize here. CANDID contains a function that injects the signal of a companion of various flux ratios and positions into the interferometric observables. Then, it derives the flux ratio at each separation over a specified percentile of position angles (we select 99%), where the detection significance level relative to a single star model equals 5σ (A. Gallenne et al. 2015). For targets with detected companions, CANDID removes the best-fit signal from the data and repeats the same process to define limits on the residual closure phases. Detection limits in terms of contrast are shown in Table 5. We then calculate the mass of an object with the parameters of the derived detection limit using the age and mass of the primary from R. J. De Rosa et al. (2014) and the MIST evolutionary models. We then convert this into a mass ratio (see Figure 1).

Importantly, CANDID assumes that errors in the interferometric observables are uncorrelated. However, interferometric observables are known to have correlated errors. J. Kammerer et al. (2020) estimated that the attainable contrast increases by a factor of 2 when estimating correlations as opposed to assuming uncorrelated errors. While assuming uncorrelated errors is a common approach to analyzing interferometric data (e.g., A. Gallenne et al. 2015; C. Lanthermann et al. 2023), it must be stated that this will only provide a conservative estimate of our limits, and does not achieve the absolute attainable contrast limit. No software is available for the CHARA array that estimates correlations within the interferometric observables, and so we proceed with our analysis, acknowledging that detection limits are conservative estimates.

3.3. Companion Population Analysis

From the sample in DF22 and this work, we observed 57 A-type stars in total at CHARA, and we detected seven companions. Three of these targets had interferometric observables that were very noisy due to a lack of sufficient calibration sources and were not included in our final demographic analysis, which includes 54 A-type primaries listed in Table 1. In our observing approach, we did not observe any dedicated calibrator stars and relied on an expected low companion frequency to then use science targets well fit by a single star model as calibrators for other science targets observed closely in time.

To characterize the companion population, we perform a Bayesian demographic analysis as in M. De Furio et al. (2022b), using PyMultiNest (F. Feroz et al. 2009; J. Buchner et al. 2014) to sample the full parameter space, maximize the likelihood

Table 3
Companion Detections

Target Name (1)	Flux Ratio (2)	Projected Sep. (mas) (3)	PA (deg) (E of N) (4)	UD_1 (mas) (5)	UD_2 (mas) (6)	$\chi^2_{\nu,1}$ (7)	$\chi^2_{\nu,2}$ (8)
HD 5448[a]	$0.01573^{+0.00039}_{-0.00042}$	64.785 0.007	144.324 0.007	0.695 0.002	⋯	1.75	1.22
HD 11636[a]	$0.13546^{+0.0011}_{-0.00089}$	63.293 0.002	102.271 0.002	1.0819 0.0008	0.549 0.007	159.5	3.18
HD 28910[a]	$0.80146^{+0.00064}_{-0.00067}$	6.102 0.0013	304.81 0.012	$0.377^{+0.007}_{-0.006}$	$0.341^{+0.008}_{-0.007}$	1332	1.17
HD 29388[a]	$0.02488^{+0.00024}_{-0.00023}$	10.126 0.002	23.59 0.02	0.553 0.005	⋯	4.39	1.14
HD 48097[a]	$0.0284^{+0.00119}_{-0.0011}$	28.145 0.007	14.16 0.02	0.288 0.015	⋯	2.26	1.51
HD 205835	0.3126 0.0006	16.631 0.001	181.55 0.006	0.5	⋯	158.13	1.75
HD 210715	0.0342 0.0003	157.296 0.006	119.07 0.012	0.5	⋯	2.37	1.48

Notes. Detected Binaries with Flux Ratio, Projected Separations in Milliarcseconds (Corrected from Absolute Wavelength Scale on MIRC-X Using the Scale Factor of 1.00535, See Section 2.2), Position Angles in Degrees, Uniform Disk Diameter of the Primary and Secondary in Milliarcseconds, and the Reduced Chi Squared Test Statistic of a Single Star Model and Binary Star Model. All detections achieved the maximum significance threshold on CANDID, 8σ.
[a] Fitted values taken from M. De Furio et al. (2022a).

Table 4
Physical Separation in au, Masses ($M_\odot$), and Mass Ratios (q)

Target Name	Physical Sep. (au)	M_{prim} ($M_\odot$)	M_{sec} ($M_\odot$)	q
HD 5448[a]	2.745 0.013	2.39	0.60	0.25
HD 11636[a]	1.156 0.013	2.01	1.05	0.52
HD 28910[a]	0.287 0.002	2.21	2.12	0.96
HD 29388[a]	0.477 0.012	2.17	0.67	0.31
HD 48097[a]	1.23 0.04	1.94	0.40	0.21
HD 205835	1.120 0.002	2.20	1.57	0.71
HD 210715	8.747 0.004	2.04	0.70	0.34

Notes. Companion masses are estimated using the MIST evolutionary models and the assumed primary mass and age from R. J. De Rosa et al. (2014), see Table 1.
[a] Fitted values taken from M. De Furio et al. (2022a) corrected using the scale factor in T. Gardner et al. (2022).

Table 5
Detection Limits

Target Name	1.0	3.0	5.0	10.0	50.0	300.0
	(mas)					
HD 1404	4.41	4.41	5.19	5.28	5.57	5.05
HD 4058	3.48	3.48	4.07	4.12	4.59	4.03
HD 14055	4.05	4.31	4.93	5.17	5.48	4.96
HD 106591	3.97	5.21	5.22	5.50	5.52	4.98
HD 118232	2.45	3.77	3.93	4.16	4.34	3.63
HD 124675	3.05	4.76	4.76	5.08	5.18	4.57
HD 125161	3.01	3.44	3.44	3.98	4.53	4.01
HD 130109	3.82	3.82	3.82	4.78	5.19	4.72
HD 141378	3.71	3.75	3.75	3.76	4.42	3.89
HD 147547	0.98	0.98	1.34	2.50	2.86	2.35
HD 152107	3.63	4.04	4.14	4.36	4.55	3.91
HD 154494	1.98	1.98	1.98	3.20	4.00	3.33
HD 156729	1.01	1.01	1.01	2.12	2.53	2.00
HD 158352	3.80	3.80	3.80	4.74	4.99	4.57
HD 165777	4.81	5.76	5.76	5.83	6.00	5.74
HD 173582	2.38	2.38	2.38	3.45	3.66	3.06
HD 173607	0.52	0.83	0.83	1.13	1.89	1.42
HD 173880	3.89	4.62	4.62	5.38	5.56	5.08
HD 174602	1.69	1.69	2.93	2.93	3.65	2.98
HD 177724	5.24	5.33	5.37	5.61	6.03	5.75
HD 184006	4.81	5.18	5.18	5.42	5.73	5.30
HD 192640	3.78	3.78	4.57	4.80	5.02	4.41
HD 199254	2.89	3.88	4.03	4.03	4.51	3.85
HD 204414	3.48	3.48	4.58	4.62	4.88	4.21
HD 205835[a]	3.58	3.58	4.18	4.18	4.72	4.41
HD 210715[a]	4.14	4.14	4.57	4.57	5.01	4.41
HD 213558	4.42	4.74	4.74	5.38	5.53	4.95

Notes. Detection Limits (Contrast in Units of Magnitudes for the H Band) Derived for Each of the New Targets in Our Sample Using MIRC-X at 1.0, 3.0, 5.0, 10.0, 50.0, and 300.0 mas in Angular Separation. We define the detection limit as the highest flux ratio companion that CANDID can recover at a given radius that is equivalent to a 5σ detection.
[a] Binary detections. Limits derived after removal of companion from data.

function, and derive posteriors for the parameters of our models. See M. De Furio et al. (2022b) for a thorough description of the analysis. We summarize our approach here. In DF22, we characterized the companion population using a frequentist approach that was sensitive over mass ratios = 0.25–1.0 and projected separations = 0.288–5.481 au. In this work, we characterize the companion population over mass ratios = 0.1–1.0 and projected separations = 0.01–27.54 au, having accounted for incompleteness in the Bayesian analysis. This allows us to place constraints over a much larger range of parameter space than previously possible.

First, we assume common functional descriptions of the mass ratio and separation distributions. We model the companion population with two models. The two-parameter model assumes a power-law fit to the mass ratio distribution and a linear flat separation distribution. The four-parameter model assumes a power-law fit to the mass ratio distribution and a lognormal fit to the separation distribution. The power-law mass ratio distribution is defined as:

$$\Phi(q) \propto \begin{cases} q^{\gamma} & \text{if } \gamma \geqslant 0 \\ (1-q)^{-\gamma} & \text{if } \gamma < 0 \end{cases} \quad (1)$$

where γ is the power-law index, and the piecewise function ensures symmetry about $q = 0.5$ as defined in C. Fontanive et al. (2019). The lognormal separation distribution is defined as:

$$\Psi(a) = \frac{1}{\sqrt{2\pi\sigma^2_{\log a}}} e^{-\frac{(\log(a)-\log(\bar{a}))^2}{2\sigma^2_{\log a}}} \quad (2)$$

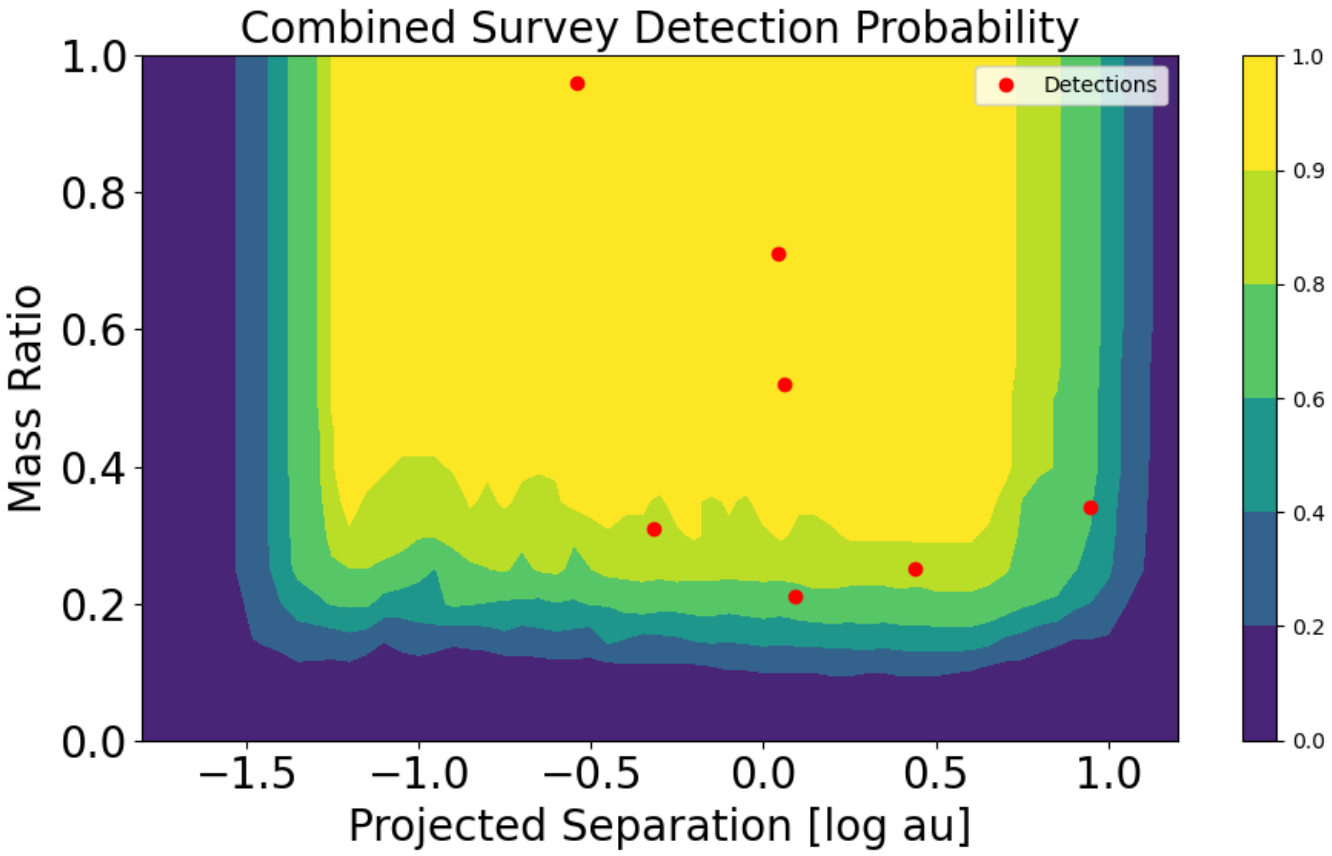

Figure 1. Summed detection probabilities for all 54 sources in our survey. Red circles show the projected separation and estimated mass ratios for all detected companions. We use this map in Section 3.3 to model the separation and mass ratio distribution of the companion population to A-type primaries within 80 pc.

where $\bar{a}$ is the mean separation and $\sigma_{\log a}$ is the standard deviation of the separation distribution in log-space.

We define the likelihood function from Poisson statistics and the physical parameters of our detected companions (C. Fontanive et al. 2018). The Poisson likelihood is:

$$\mathcal{L}_p = \frac{k^d e^{-k}}{d!} \tag{3}$$

where k is the expected number of companion detections given the model and d is the number of true observed companions. The expected number of detections is defined as:

$$k = \sum_{i=1}^{n} p_i * \mathrm{CF} * \frac{N}{n} \tag{4}$$

where CF is the companion frequency of the sample over mass ratios = 0.1–1 and 0.01–27.54 au, N is the total number of sources in our sample (here 54), n is the total number of generated companions in the artificial population sampling process, and p_i is the probability that the i generated companion will be detected given our survey sensitivity. We constructed the detection probability map by summing over the detection limits of each source in our sample, which produces the average sensitivity of the whole survey (see Figure 1). Due to the different distances to our sources, the inner and outer working angles are not the same in terms of physical separation for each source, and therefore, there is a gradient of sensitivity up to the region of common sensitivity of all sources. We then assign p_i from this map as the probability that the generated companions would be detected, given their physical parameters.

We assume flat priors for $-5.0 < \gamma < 5.0$ and $0.0 <$ CF < 1.0 and log-flat priors for $0.0 < \log(a_o) < 4.0$ and $0.1 < \sigma_{\log a} < 5.0$ so that each au is equally weighted. Then, we generate the mass ratio and projected orbital separation distributions of Equations (1) and (2) based on each sampled value. From each model, we generate $n = 10^4$ companions, with mass ratios = 0.1–1 and projected orbital separations = 0.01–27.54 au, and calculate p_i for each companion. We then sum over all n generated companions to evaluate k, and compute the Poisson likelihood where CF is a free parameter.

We also calculate the likelihood of the model given the physical parameters of our real detections. First, we generate the model of the population and convolve it with the combined survey detection probability to make a joint probability distribution that gives the expected companion distribution based on the sampled model and the sensitivity of the survey. Finally, we evaluate the joint probability of each true detection, p_j, based on its derived physical parameters. The total likelihood is calculated as:

$$\mathcal{L} = \mathcal{L}_p * \prod_{j=1}^{d} p_j. \tag{5}$$

From our sample of 54 A-type primaries, we estimated the following four parameters over mass ratios = 0.1–1.0 and projected separation 0.01–27.54 au with 1σ errors

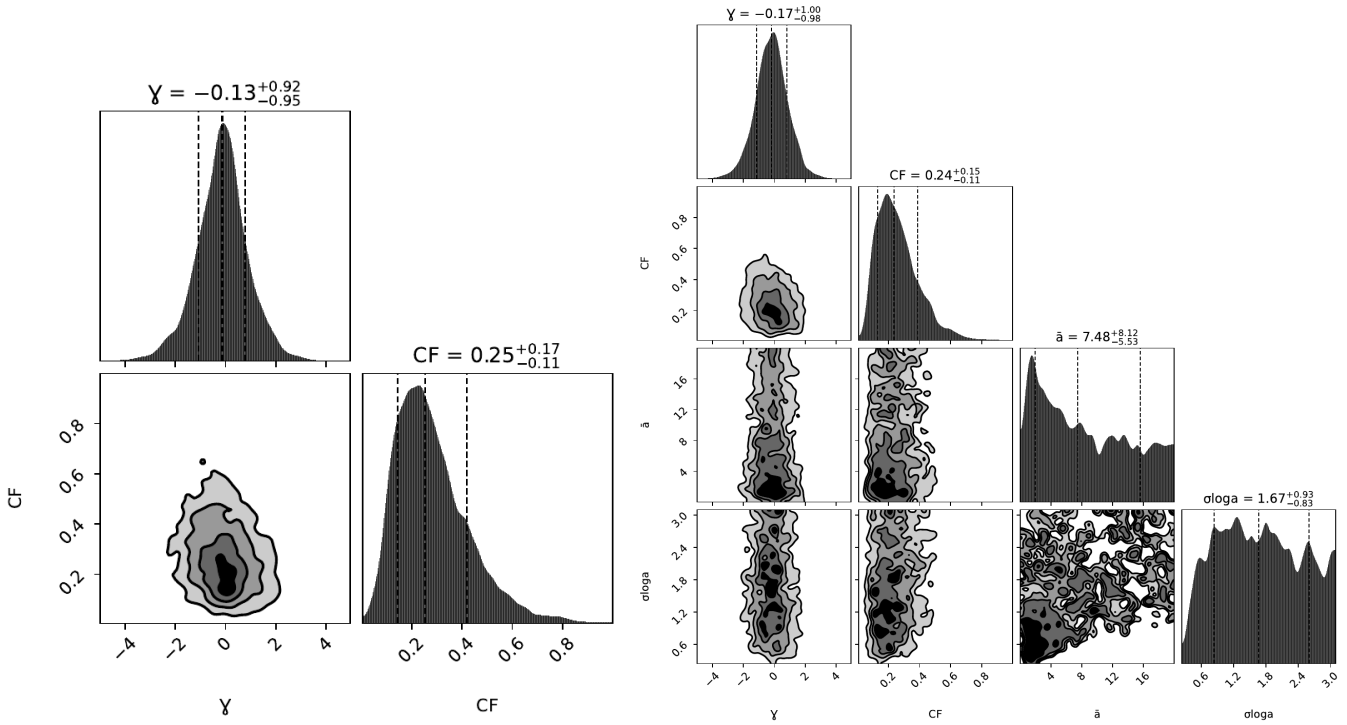

Figure 2. Corner plots representing the posterior distributions of the companion population model used in our fit. γ is the exponent to the power-law model of the mass ratio distribution, CF is the companion frequency over $q = 0.1$–1 and $a = 0.01$–27.54 au, $\bar{a}$ is the mean separation of the lognormal separation distribution in units of au, and $\sigma_{\log(a)}$ is the standard deviation of the lognormal separation distribution. The separation distribution is unconstrained with a lognormal, likely due to the low number of detections in our survey.

(68% confidence interval): $\gamma = -0.17^{+1.00}_{-0.98}$, CF $= 0.24^{+0.15}_{-0.11}$, $\bar{a} = 7.48^{+8.12}_{-5.53}$ au, and $\sigma_{\log a} = 1.67^{+0.93}_{-0.83}$. As shown in Figure 2, the parameters of the projected orbital separation distribution are unconstrained, likely due to the low number of detections in our sample. For the two-parameter model, we find: $\gamma = -0.13^{+0.92}_{-0.95}$, CF $= 0.25^{+0.17}_{-0.11}$. Between these two models, the difference in the Bayesian evidence is 0.2. Therefore, the comparison is inconclusive, and we draw no distinction between the two models. This allows us to conclude that the observed companion population is not better modeled by a lognormal distribution fit compared to a flat separation distribution. This is potentially due to the low number of detections or that the underlying separation distribution is wide, and that our survey over 0.01–27.54 au (3.44 units in log-separation) does not sample enough of the distribution to constrain the underlying model. We use the two-parameter model for further analysis.

4. Discussion

Our total source list was derived from the R. J. De Rosa et al. (2014) VAST sample. We excluded sources with known Ap or Am spectral types in order to have a sample of chemically typical A-type stars, but did not make sample selections based on previously detected companions. These exclusions may have an impact due to their different spin rate than typical A-type stars, but evidence has been found for an increase in companion frequency for both slow rotators (C. L. Smith et al. 2024) and fast rotators (M. Kounkel et al. 2023). Therefore, these results should be interpreted for the population of chemically typical A-type stars. Sources were then randomly selected based on the observing nights allocated. Both additional binary detections in this work were previously targeted for companion search through adaptive optics imaging and common proper motion analysis. Only one was found to have a companion over separations sampled, HD 205835, at a separation of 454 au and a mass ratio of 0.05. Therefore, this is a triple system with a close binary pair separated by 1.12 au and a widely separated low-mass tertiary, a common configuration for triples. HD 205835 was observed from 32 to 794 au and 3980 to 45,000 au. HD 210715 was observed from 32 to 794 au.

4.1. Comparing the Companion Population to Models

4.1.1. Mass Ratio Distribution

We derived a best-fit power-law index of $-0.13^{+0.92}_{-0.95}$ to the mass ratio distribution for the close companions to A-stars. The R. J. De Rosa et al. (2014) multiplicity survey of A-type stars is sensitive to companions beyond 20 au and mass ratios $\geqslant$0.15 for a majority of their sample. For companions between 30–125 au and 125–800 au, they describe the mass ratio distribution as a power law with a best-fit index $\gamma = -0.5^{+1.2}_{-1.0}$ and $-2.3^{+1.0}_{-0.9}$, respectively. Our results are consistent with both of these power-law fits, given the relatively large errors in their estimate and in our own. A future expansion of this survey would allow for a larger sample of detected companions, which would greatly reduce errors on the power-law index to the mass ratio distribution.

4.1.2. Companion Frequency

S. J. Murphy et al. (2018) conducted a survey of Scuti variable stars using the phase modulation technique on Kepler light curves and found a CF = 0.139 0.021 over 0.6–3.6 au and all mass ratios. Roughly 70% of their companions have

Table 6
Companion Population Parameters and Sensitivities of Each Tested Model with the Resulting Statistics

Primary Spectral Type	γ	$\log(a_o)$	$\sigma_{\log a}$	CF	$\log(a)$ Sensitivity	q Sensitivity	Expected CF	Posterior Probability
FGK-type[a]	0	1.7	1.68	0.61 0.02	$-2 \leqslant \log(a) \leqslant 4$	$q \geqslant 0.1$	0.29 0.01	0.53
A-type[b]	$-0.5^{+1.2}_{-1.0}$	2.59 0.13	0.79 0.12	0.219 0.026	$1.5 \leqslant \log(a) \leqslant 2.9$	$q \geqslant 0.1$	$0.028^{+0.018}_{-0.014}$	0.005
B-type[c]	−0.46 0.14	1.05 0.2	1.35 0.2	1.35 0.20	$-2 \leqslant \log(a) \leqslant 4$	$q \geqslant 0.1$	$0.70^{+0.14}_{-0.13}$	0.04

Notes.
[a] D. Raghavan et al. (2010).
[b] R. J. De Rosa et al. (2014).
[c] A. C. Rizzuto et al. (2013).

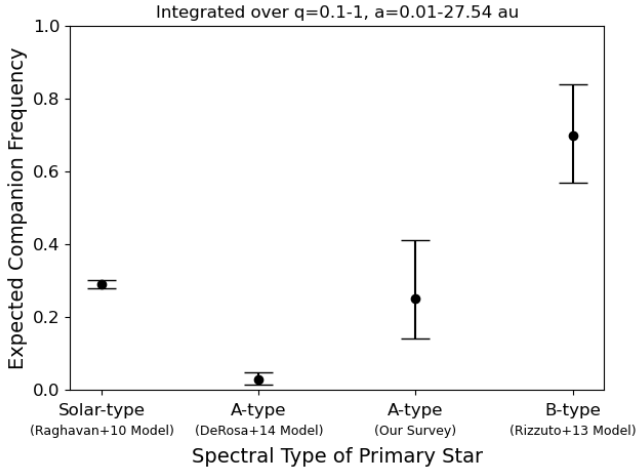

Figure 3. Companion frequencies based on the spectral type of the primary star from the various models listed in Section 4.1.2. All frequencies are calculated over mass ratios = 0.1–1.0 and separations (a) = 0.01–27.54 au. The companion frequency for Solar-type primaries is derived from the model of D. Raghavan et al. (2010), A-type primaries from the model of R. J. De Rosa et al. (2014), and this survey, and B-type primaries from the model of A. C. Rizzuto et al. (2013).

mass ratios = 0.2–1.0, resulting in a CF = 0.10 0.021 over those mass ratios and separations. In our full sample, we detect four companions out of the 54 sources over the same mass ratios and separations, resulting in a CF = $0.07^{+0.05}_{-0.02}$ consistent with the S. J. Murphy et al. (2018) result.

Other surveys have attempted to characterize the companion frequency of A-type stars using LBI with VLTI/Gravity and common proper motion analyses (I. Waisberg et al. 2023). However, they only analyzed stars with high accelerations between epochs of Hipparcos and Gaia, which introduces a significant bias in their sample. All high acceleration stars should have a companion over the parameter space sampled, and cannot be representative of the A-type population itself. Therefore, we cannot compare our results to their estimated companion frequency, which is heavily biased toward the presence of companions.

Other surveys have characterized the companion population to various types of primary stars. D. Raghavan et al. (2010) characterized the companion population to Galactic field FGK stars over all separations, R. J. De Rosa et al. (2014) to field A-type stars with adaptive optics beyond 20 au, and A. C. Rizzuto et al. (2013) to B-type stars in Sco-Cen over nearly all separations. These surveys each fit the mass ratio and separation distributions with a power law and a lognormal function, respectively. We use Equations (1) and (2) to define the mass ratio and separation distributions and integrate these functions over the sensitivity of our own survey using the stated values of the parameters from past studies to estimate the expected companion frequency for each of these types of primary stars:

$$\mathrm{CF} = C_n * \int_{q1}^{q2} \Phi(q)dq \int_{a1}^{a2} \Psi(a)da \quad (6)$$

We first integrate these functions over the sensitivity of their own survey sampling the values of CF, γ, $\sigma_{\log a}$, and $\overline{a}$ 10^5 times, see Table 6. Each evaluation of Equation (6) allows us to solve for C_n which we then input back into the same equation, but this time integrating over the sensitivity of our survey in this work, q = 0.1–1.0 and a = 0.01–27.54 au, to arrive at a value for CF, see Figure 3. We lastly evaluate the posterior probability that the expected CF of each of these surveys over our sensitivity is the same as that of our survey. We integrate the posterior distribution of the companion frequency from our two-parameter model, see Figure 2, from 0 to the CF of each sampling stated above for the A-type model and from the CF of each sampling to infinity for the FGK- and B-type models. This ensures that the correct tail of the posterior distribution is evaluated to determine the posterior probability that the model can describe our observations of A-stars. In Table 6, we present the estimated posterior probabilities for the companion population models to solar-type, A-type, and B-type primaries, which are 0.53, 0.005, and 0.04, respectively. From these results, we find that: (a) there is no evidence for a difference between the multiple population of our A-type sample and that of solar-type stars as found in DF22, (b) the companion frequency for A-type stars at closer separations is higher than if extrapolating the R. J. De Rosa et al. (2014) lognormal separation distribution which should apply for separations greater than roughly 100 au where they are mostly complete, and (c) the companion frequency to B-type primaries is potentially larger than A-type primaries over mass ratios and separations sampled which was not found in DF22 due to the low sample size and much more stringently probed parameter space utilizing the frequentist approach.

4.2. Implications

Our analysis of 54 chemically typical A-type stars within 80 pc observed with long-baseline interferometry reveals a companion frequency of $0.25^{+0.17}_{-0.11}$ over mass ratios 0.1–1.0 and projected separations 0.01–27.54 au. As in DF22, we find that extrapolating the companion population model of R. J. De Rosa et al. (2014) cannot reproduce our observed results, see Figure 3. The best-fit power-law index to the mass ratio

distribution shows hints that it is consistent with the close companion population from R. J. De Rosa et al. (2014), but we cannot rule out the power-law index of the wide companion population, which is within 2σ. We do not find any difference between the companion frequency of solar-type stars in the field (D. Raghavan et al. 2010) and our sample of A-type stars, over mass ratios = 0.1–1.0 and projected separations = 0.01–27.54 au. However, we calculate a probability of 0.04 that the companion population of B-type stars can describe the observations of the companion population of our A-star sample due to the abundance of close-in companions to B-type primaries. See Table 6 and Figure 3 for a comparison to other surveys on the sensitivity of our survey.

It is well established in the literature that more massive stars have a higher companion frequency, and that there is a break in the separation distributions: low-mass and solar-type stars follow a lognormal with increasingly fewer companions at closer separations, whereas high companion frequencies of high-mass stars continue toward closer separations (M. Moe & R. Di Stefano 2017). However, the trend in the companion frequency at close separations is unclear for A-type primaries. Our results suggest that intermediate-mass A-type binaries are more like solar-type stars and have similar formation pathways. Primaries with $M \gtrsim 3M_{\odot}$ (O and B stars) follow similar distributions to more massive stars. This break could be consistent with an enhanced role for disk fragmentation only for high-mass primaries, which is consistent with theoretical predictions (K. M. Kratter & C. D. Matzner 2006). Numerical simulations are able to reproduce even close-in low-mass binaries through turbulent fragmentation coupled with migration and dynamical interactions (M. R. Bate 2018). Similarly, large star formation simulations like STARFORGE, which better sample the IMF (M. Y. Grudić et al. 2022; D. Guszejnov et al. 2023), are able to recover the multiplicity properties of low-mass stars reasonably well despite not having resolved protostellar disks. However, they somewhat underproduce companions at higher masses, perhaps due to the lack of resolved disk fragmentation. Note that there remain uncertainties in how to compare the simulated and observed companion fractions due to incompleteness at the lowest masses, and thus mass ratios, as well as closest separations. Ultimately, with a larger sample of A-type stars, we will be able to explore differences in the companion population as a function of primary mass and differentiate between potential formation mechanisms through the derived mass ratio distribution.

5. Conclusion

We have conducted a multiplicity survey of 54 nearby, chemically typical A-type stars within 80 pc using long-baseline interferometry at the CHARA Array with the MIRC-X and MYSTIC instruments. To summarize the results of our survey:

(1) We detected seven companions in total, two from the newest data, with projected separations 6–158 mas (0.287–8.747 au) and mass ratios = 0.21–0.96. For our sample of A-type stars with masses of 1.44–2.93$M_{\odot}$, we observed a completeness-corrected companion frequency of $0.25^{+0.17}_{-0.11}$ over the sensitivity of our survey, mass ratios 0.1–1.0, and projected separations 0.01–27.54 au.

(2) Our results are consistent with what we had previously found in DF22, except now characterized over a much larger range in parameter space due to the inclusion of a Bayesian demographic analysis.

(3) Our estimate of the companion frequency is consistent with that of FGK-type stars over the sensitivity sampled, but we find a probability of 0.04 that the B-type companion population model can replicate our observed companion frequency to A-type primaries over the sensitivity of our survey. This may be indicative of an increased occurrence of companions to B-type stars ($\gtrsim 2.5M_{\odot}$), potentially due to a higher incidence of disk fragmentation.

Acknowledgments

This work is based upon observations obtained with the Georgia State University Center for High Angular Resolution Astronomy Array at Mount Wilson Observatory. The CHARA Array is supported by the National Science Foundation under grant No. AST-2034336 and AST-2407956. Institutional support has been provided from the GSU College of Arts and Sciences and the GSU Office of the Vice President for Research and Economic Development. Time at the CHARA Array was granted through the NOIRLab community access program (NOIRLab PropID: 2020B-0290; PI: M. De Furio). MIRC-X received funding from the European Research Council (ERC) under the European Union's Horizon 2020 research and innovation program (grant No. 639889). S.K. acknowledges funding for MIRC-X received from the European Research Council (ERC) under the European Union's Horizon 2020 research and innovation program (Starting grant No. 639889 and Consolidated grant No. 101003096). J.D.M. acknowledges funding for the development of MIRC-X (NASA-XRP NNX16AD43G, NSF-AST 2009489) and MYSTIC (NSF-ATI 1506540, NSF-AST 1909165). This research has made use of the Jean-Marie Mariotti Center `Aspro` service, available at http://www.jmmc.fr/aspro. This research has made use of the Jean-Marie Mariotti Center `SearchCal` service, which involves the JSDC and JMDC catalogs, available at https://www.jmmc.fr/searchcal. This work has made use of data from the European Space Agency (ESA) mission Gaia (https://www.cosmos.esa.int/gaia), processed by the Gaia Data Processing and Analysis Consortium (DPAC, https://www.cosmos.esa.int/web/gaia/dpac/consortium). Funding for the DPAC has been provided by national institutions, in particular the institutions participating in the Gaia Multilateral Agreement. M.D.F. is supported by an NSF Astronomy and Astrophysics Postdoctoral Fellowship under award AST-2303911. M.D.F. acknowledges S.F. K. M.K. acknowledges support from the NSF AAG program under award 2407522.

ORCID iDs

Matthew De Furio https://orcid.org/0000-0003-1863-4960
Tyler Gardner https://orcid.org/0000-0002-3003-3183
John D. Monnier https://orcid.org/0000-0002-3380-3307
Michael R. Meyer https://orcid.org/0000-0003-1227-3084
Kaitlin M. Kratter https://orcid.org/0000-0001-5253-1338
Cyprien Lanthermann https://orcid.org/0000-0001-9745-5834
Narsireddy Anugu https://orcid.org/0000-0002-2208-6541
Stefan Kraus https://orcid.org/0000-0001-6017-8773
Benjamin R. Setterholm https://orcid.org/0000-0001-5980-0246

References

Abt, H. A. 1965, ApJS, 11, 429
Adams, F. C., Ruden, S. P., & Shu, F. H. 1989, ApJ, 347, 959
Anugu, N., Le Bouquin, J.-B., Monnier, J. D., et al. 2020, AJ, 160, 158
Babusiaux, C., Fabricius, C., Khanna, S., et al. 2023, A&A, 674, A32
Bate, M. R. 2018, MNRAS, 475, 5618
Bate, M. R., Bonnell, I. A., & Bromm, V. 2002, MNRAS, 336, 705
Bate, M. R., Bonnell, I. A., & Bromm, V. 2003, MNRAS, 339, 577
Bonnell, I. A., & Bate, M. R. 1994, MNRAS, 269, L45
Bourges, L., Mella, G., Lafrasse, S., et al. 2017, yCat, 2346
Buchner, J., Georgakakis, A., Nandra, K., et al. 2014, A&A, 564, A125
Carquillat, J. M., & Prieur, J. L. 2007, MNRAS, 380, 1064
Che, X., Monnier, J. D., Zhao, M., et al. 2011, ApJ, 732, 68
Chelli, A., Duvert, G., Bourgès, L., et al. 2016, A&A, 589, A112
Choi, J., Dotter, A., Conroy, C., et al. 2016, ApJ, 823, 102
De Furio, M., Gardner, T., Monnier, J., et al. 2022a, ApJ, 941, 118
De Furio, M., Liu, C., Meyer, M. R., et al. 2022b, ApJ, 941, 161
De Rosa, R. J., Patience, J., Wilson, P. A., et al. 2014, MNRAS, 437, 1216
Dotter, A. 2016, ApJS, 222, 8
ESA 1997, The HIPPARCOS and TYCHO Catalogues (Noordwijk: ESA)
Feroz, F., Hobson, M. P., & Bridges, M. 2009, MNRAS, 398, 1601
Fontanive, C., Biller, B., Bonavita, M., & Allers, K. 2018, MNRAS, 479, 2702
Fontanive, C., Rice, K., Bonavita, M., et al. 2019, MNRAS, 485, 4967
Gaia Collaboration 2022, yCat, 1355
Gaia Collaboration, Arenou, F., Babusiaux, C., et al. 2023, A&A, 674, A34
Gaia Collaboration, Prusti, T., de Bruijne, J., H., J., et al. 2016, A&A, 595, A1
Gallenne, A., Mérand, A., Kervella, P., et al. 2015, A&A, 579, A68
Gardner, T., Monnier, J. D., Fekel, F. C., et al. 2021, AJ, 161, 40
Gardner, T., Monnier, J. D., Fekel, F. C., et al. 2022, AJ, 164, 184
Goodwin, S. P., Whitworth, A. P., & Ward-Thompson, D. 2004, A&A, 414, 633
Grudić, M. Y., Guszejnov, D., Offner, S. S. R., et al. 2022, MNRAS, 512, 216
Guszejnov, D., Raju, A. N., Offner, S. S. R., et al. 2023, MNRAS, 518, 4693
Holl, B., Sozzetti, A., Sahlmann, J., et al. 2023, A&A, 674, A10
Janson, M., Hormuth, F., Bergfors, C., et al. 2012, ApJ, 754, 44
Jennison, R. C. 1958, MNRAS, 118, 276
Kammerer, J., Mérand, A., Ireland, M. J., & Lacour, S. 2020, A&A, 644, A110
Kervella, P., Arenou, F., Mignard, F., & Thévenin, F. 2019, A&A, 623, A72
Kervella, P., Arenou, F., & Thévenin, F. 2022, A&A, 657, A7
Kounkel, M., Stassun, K. G., Hillenbrand, L. A., et al. 2023, AJ, 165, 182
Kratter, K. M., & Matzner, C. D. 2006, MNRAS, 373, 1563
Kraus, A. L., Ireland, M. J., Huber, D., Mann, A. W., & Dupuy, T. J. 2016, AJ, 152, 8
Lanthermann, C., Le Bouquin, J. B., Sana, H., et al. 2023, A&A, 672, A6
Moe, M., & Di Stefano, R. 2017, ApJS, 230, 15
Moe, M., & Kratter, K. M. 2021, MNRAS, 507, 3593
Monnier, J. D. 2000, in Principles of Long Baseline Stellar Interferometry, ed. P. R. Lawson (Washington, DC: NASA), 203
Monnier, J. D., Che, X., Zhao, M., et al. 2012, ApJL, 761, L3
Monnier, J. D., Le Bouquin, J.-B., Anugu, N., et al. 2018, Proc. SPIE, 10701, 1070122
Monnier, J. D., Pedretti, E., Thureau, N., et al. 2006, Proc. SPIE, 6268, 62681P
Monnier, J. D., Traub, W. A., Schloerb, F. P., et al. 2004, ApJL, 602, L57
Monnier, J. D., Zhao, M., Pedretti, E., et al. 2007, Sci, 317, 342
Murphy, S. J., Moe, M., Kurtz, D. W., et al. 2018, MNRAS, 474, 4322
Offner, S. S. R., Kratter, K. M., Matzner, C. D., Krumholz, M. R., & Klein, R. I. 2010, ApJ, 725, 1485
Offner, S. S. R., Moe, M., Kratter, K. M., et al. 2023, in ASP Conf. Ser. 534, Protostars and Planets VII, ed. S. Inutsuka et al. (San Francisco, CA: ASP), 275
Paxton, B., Bildsten, L., Dotter, A., et al. 2011, ApJS, 192, 3
Paxton, B., Cantiello, M., Arras, P., et al. 2013, ApJS, 208, 4
Paxton, B., Marchant, P., Schwab, J., et al. 2015, ApJS, 220, 15
Paxton, B., Schwab, J., Bauer, E. B., et al. 2018, ApJS, 234, 34
Pourbaix, D. 2000, A&AS, 145, 215
Raghavan, D., McAlister, H. A., Henry, T. J., et al. 2010, ApJS, 190, 1
Reid, I. N., Lewitus, E., Allen, P. R., Cruz, K. L., & Burgasser, A. J. 2006, AJ, 132, 891
Rizzuto, A. C., Ireland, M. J., Robertson, J. G., et al. 2013, MNRAS, 436, 1694
Rogers, A. E. E., Hinteregger, H. F., Whitney, A. R., et al. 1974, ApJ, 193, 293
Sana, H., de Mink, S. E., de Koter, A., et al. 2012, Sci, 337, 444
Setterholm, B. R., Monnier, J. D., Le Bouquin, J.-B., et al. 2023, JATIS, 9, 025006
Smith, C. L., Moe, M., & Kratter, K. M. 2024, ApJ, 975, 153
Susemiehl, N., & Meyer, M. R. 2022, A&A, 657, A48
Swihart, S. J., Garcia, E. V., Stassun, K. G., et al. 2017, AJ, 153, 16
ten Brummelaar, T. A., Gies, D. G., McAlister, H. A., et al. 2016, Proc. SPIE, 9907, 990703
ten Brummelaar, T. A., McAlister, H. A., Ridgway, S. T., et al. 2005, ApJ, 628, 453
Waisberg, I., Klein, Y., & Katz, B. 2023, MNRAS, 521, 5232
Winters, J. G., Henry, T. J., Jao, W.-C., et al. 2019, AJ, 157, 216
Young, M. D., & Clarke, C. J. 2015, MNRAS, 452, 3085
Zhao, M., Monnier, J. D., Pedretti, E., et al. 2009, ApJ, 701, 209